X-ray structure analysis on alkali metals adsorbed on Ge(001)(2×1)

H. L. Meyerheim, R. Sawitzki, and W. Moritz
Institut für Kristallographie und Mineralogie, Universität München, Theresienstrasse 41, 80333 München, Germany
(Received 31 March 1995)

Surface x-ray diffraction has been used to investigate the geometric structure of Cs, K, and Na adsorbed on Ge(001)(2×1) at room temperature. At low and saturation coverage corresponding to about 0.3 monolayer (ML) and 0.6–0.7 ML, respectively (1 ML=6.25×10^{14} atoms cm^{-2}), adsorption takes place in the large grooves between the Ge-dimer atoms. For all adsorption systems investigated, the statistical occupation of two different sites is observed: first, above the third-layer Ge atoms ($T3$), and second, in an asymmetric site close to the dangling bonds of the Ge-dimer atoms (a-$T4$). At about half saturation coverage we have evidence for the preferential occupation of the adsorption site $T3$ indicating a coverage-dependent ordering and the formation of a linear densely packed chain along the [110] direction of the substrate. Whereas the bond lengths of the $T3$-adsorbed alkali metals to nearest-neighbor Ge atoms are in the regime found for bulk alkali-metal–Ge structures, which can be interpreted as indicative of covalent bonding, they are shorter for alkali metals adsorbed in a-$T4$ to the Ge-dimer atoms, where average distances in the regime between covalent and ionic bonding are observed. This can be interpreted by partial charge transfer to the empty dangling bond states. The alkali metals Cs and K are generally found to occupy different adsorption heights, which can be related to a strong disorder normal to the surface due to steric reasons. This is not observed for the smaller Na atoms. Generally, the Ge-dimer bond length (2.45 Å) and the dimer asymmetry (inclination angle of the dimer bond to the surface ±17.6°) are not influenced by alkali-metal adsorption within 0.1 Å and about 4°, respectively. Shifts of Ge atoms at least down to the fourth layer below the surface are observed.

I. INTRODUCTION

Alkali-metal (AM) adsorption has played an important role in surface science from theoretical, experimental, and technological points of view.[1–3] This is because AM's have simple electronic structures and are interesting candidates for the study of chemisorption. In addition, AM adsorption induces the lowering of the substrate work function and is a promoter of surface chemical reactions. Despite the simplicity of the AM electronic structure, adsorption on metals and semiconductors has turned out to be a very complicated matter, which in many aspects is still under dispute. The lowering of the substrate work function has been interpreted in terms of the Gurney model,[4] suggesting charge transfer from the AM to the (metal) substrate; on the basis of experimental[5] and theoretical[6,7] work this has been questioned supporting the picture of a polarized covalent bond. However, new theoretical investigations[8–10] again favor the ionic picture at low coverages. For AM adsorption on semiconductors the question whether the surface is metallized upon AM adsorption is also under discussion. This is intimately correlated with the geometric structure of the AM-covered surface.

Figure 1 schematically shows a side and a top view of the clean Si(001) and Ge(001) surfaces. The formation of dimers on the surface leads to the well-known (2×1) reconstruction. For Ge(001)(2×1) asymmetric dimers were observed using different experimental techniques such as scanning tunneling microscopy[11] (STM) and x-ray diffraction (XRD).[12] The dimer asymmetry can be static or dynamic in nature; the latter has been suggested for Si(001)(2×1) by Dabrowski and Scheffler[13] and is in agreement with recent theoretical investigations[14] that conclude that in contrast to Si(001)(2×1) the dimer flipping is strongly suppressed for Ge(001)(2×1). In the lower part of Fig. 1 the Ge(001)(2×1) unit cell (a_0=8.000 Å, b_0=4.000 Å) is indicated by the dashed line, where large and small circles represent the dimer atoms and second-layer Ge atoms, respectively. High-symmetry AM adsorption sites are labeled by P (pedestrial), T (top), D (dimer-bridge), $T3$ (top third layer), and $T4$ (top fourth layer), where both $T3$ and $T4$ are often referred to as "cave sites" leading to some confusion in the literature. All adsorption sites have been proposed on the basis of experimental and theoretical investigations. Table I gives an overview of some investigations that were carried out at different AM coverages.[15–39] Besides the occupation of only a single adsorption site also the combination of two positions such as $P/T3$, $P/T4$, and $T3/T4$ ("double-layer models") has been suggested at AM saturation coverage, which generally is supposed to be about 1 monolayer (ML) in the literature.[40–42] 1 ML corresponds to 6.25×10^{14} atoms cm^{-2}, which is equivalent to two AM atoms per (2×1) substrate unit cell. However, as will be shown in the later discussion of our x-ray experiments, the saturation coverage is found to be in the regime between 0.6 and 0.7 ML. Using angular-resolved ultraviolet photoelectron spectroscopy (ARUPS) Enta *et al.*[20] determined for the double-layer model $P/T3$ the Si(001) surface to be insulating. The double-layer models are in disagreement with the adsor-

bate structure originally proposed by Levine[15] in which AM adsorption in the *P* site is assumed only. This structure model corresponds to a metallic surface and to a saturation coverage of 0.5 ML.

It should be noted that the majority of the investigations listed in Table I deals with the AM/Si(001) adsorption system and only a recent x-ray standing-wave (XSW) experiment on K/Ge(001)(2×1) uses a Ge substrate.[26] This should be kept in mind when comparing our results with previous work. However, a very similar behavior of the Cs/Si(001)(2×1) and the Cs/Ge(001)(2×1) systems has been observed by Lin, Miller, and Chiang[43] using x-ray photoelectron spectroscopy (XPS). In addition, a close similarity of the AM/Ge and AM/Si adsorption systems from a structural point of view can be inferred from the fact that the bulk structures of cubic AMGe and AMSi (AM=K,Rb,Cs) as well as those of K_8Ge_{46} and K_8Si_{46} are isotypic.[44,45]

Direct experimental evidence for the AM adsorbate structures listed in Table I is rare. For example, Auger-electron diffraction[27] (AED) and photoelectron diffraction[21] (XPD) make use of the strong forward scattering of the electrons by an intervening atom making a "triangulation" procedure necessary. Low-energy electron diffraction (LEED) has also been used for the adsorption site determination. On the basis of their beam intensity versus electron curves Urano *et al.*[17,18] concluded-

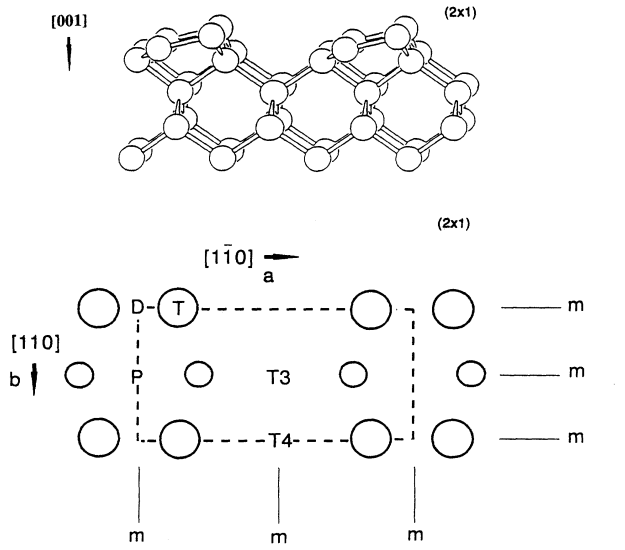

FIG. 1. Structure of the (2×1) reconstructed (001) surfaces of Si and Ge in perspective (upper part) and top view (lower part). The (2×1) unit cell is indicated by the dashed line. Mirror lines for the projected structure are represented by the solid lines and are labeled by *m*. Large and small circles represent first-layer dimer atoms and second-layer atoms, respectively. High-symmetry AM adsorption sites are labeled by *D*, *T*, *P*, *T*3, and *T*4.

TABLE I. High-symmetry adsorption sites of Na, K, and Cs on the (2×1) reconstructed surfaces of Si(001) and Ge(001) as proposed on the basis of various experimental and theoretical investigations (Refs. 15–39). UPS denotes ultraviolet photoemission spectroscopy. PAX denotes the photoemission of adsorbed xenon. FI-STM denotes field ion STM. RHEED denotes reflection high-energy electron diffraction. PEXAFS denotes photoemission extended x-ray-absorption fine structure. MEIS denotes medium energy ion scattering. TDS denotes thermal desorption spectroscopy.

	P	*T*3	*T*4	*T*	*P*/*T*3	*P*/*T*4	*T*3/*T*4
			Experiment				
LEED	Ref. 15				Ref. 17		
	Ref. 16				Ref. 18		
ARUPS					Ref. 19		
					Ref. 20		
XPD					Ref. 21		
STM			Ref. 22	Ref. 23			
XPS			Ref. 22				
UPS			Ref. 22				
PAX							Ref. 24
TDS							Ref. 24
XSW			Ref. 25			Ref. 25	
			Ref. 26				
AED		Ref. 27					
FI-STM		Ref. 28		Ref. 29			
RHEED					Ref. 30		
MEIS/AES					Ref. 31	Ref. 31	
PEXAFS			Ref. 32				
			Theory				
	Ref. 33		Ref. 34				
	Ref. 36		Ref. 35				
		Ref. 37			Ref. 37		
			Ref. 32		Ref. 38		
		Ref. 39			Ref. 39		

ed the double-layer model ($P/T3$) to be most likely at AM saturation coverage; however, the differences to the reliability factors obtained for single adsorption site structure models were small. One major advantage of XRD as compared to LEED is that in most cases XRD data can be interpreted in terms of the kinematic diffraction theory. Therefore, it is capable of the analysis of even complicated adsorbate structures and a number of experiments have been performed so far.[46] However, in many cases only "in-plane" reflections ($hk0$) have been analyzed, allowing the determination of the projected structure only.

In contrast, our diffractometer[47] allows the measurement of reflections related to large momentum transfers q_z normal to the sample surface making a depth resolved analysis of the superstructure possible. In a recent work[48] we have reported on some results of our investigation on Cs/Ge(001)(2×1) at about half Cs-saturation coverage. In the present paper we focus in more detail on the coverage dependence of the adsorbate structures and on a comparative study of the adsorption geometry of Na, K, and Cs on Ge(001)(2×1).

In general, the AM/Ge(001)(2×1) adsorbate geometries are found to be similar. Evidence for a coverage dependence of the adsorption geometry is given that might be related to previous STM work of Soukiassian *et al.*[22]

II. EXPERIMENT

The experiments were performed using an ultrahigh-vacuum (UHV) diffractometer described earlier.[47] For the XRD investigations on Cs/Ge(001)(2×1) the x-ray source was an 18-kW rotating anode equipped with a pyrolytic graphite monochromator selecting Cu-$K\alpha$ radiation. All other experiments were performed at the W1 wiggler beam line of the Hamburger Synchrotron Radiation Laboratory (HASYLAB) using an x-ray wavelength of $\lambda = 1.166$ Å. Prior to mounting into the UHV chamber the Ge(001) crystal ($10 \times 15 \times 1$ mm^3) was chemomechanically polished using diamond paste and a 12% NaClO solution. Final cleaning was achieved in UHV (base pressure $\approx 1 \times 10^{-10}$ mbar) by repeated cycles of Ar^+-ion sputtering (500 eV) and subsequent annealing up to 650 °C followed by slow cooling to room temperature. High sample quality could be achieved by this procedure. Using the rotating anode x-ray source we measured for the in-plane ($\frac{3}{2}0$) superlattice reflection[49] of the clean Ge(001)(2×1) surface a peak count rate of 54/s and a full width at half maximum (FWHM) of about 0.3°, which is about the resolution limit under laboratory conditions. For comparison, the count rate using the synchrotron source was larger by about two orders of magnitude and a FWHM of 0.25° ($\approx 1.03 \times 10^{-2}$ Å^{-1}) was obtained that is related to a terrace width on the order of

TABLE II. Observed in-plane structure factor intensities $|F^{obs}|^2$ and corresponding standard deviations σ for the clean and Cs-covered Ge(001)(2×1) surface. The intensities are normalized to the (30) reflection. For the AM/Ge(001)(2×1) systems the calculated intensities $|F^{cal}|^2$ for the best structure models are listed for comparison. The reflection indices are related to the (2×1) superstructure unit cell.

	Ge(001)(2×1) Grey *et al.* (Ref. 50) Synchrotron		Cs/Ge(001) (2×1) superstructure ≈0.27 ML			≈0.38 ML Rotating anode			≈0.60 ML		
hk	$\|F^{obs}\|^2$	σ	$\|F^{obs}\|^2$	σ	$\|F^{cal}\|^2$	$\|F^{obs}\|^2$	σ	$\|F^{cal}\|^2$	$\|F^{obs}\|^2$	σ	$\|F^{cal}\|^2$
1 0	45.6	1.5	10.0	0.6	10.6	1.0	0.2	1.0	2.7	0.7	2.6
3 0	100.0	4.4	100.0	6.0	103.3	100.0	5.0	93.3	100.0	8.0	99.2
5 0	2.6	1.2	5.7	2.0	4.9				2.6	1.8	1.0
7 0	4.7	2.1	7.1	5.7	12.0	2.5	2.4	1.8			
9 0	1.5	1.5									
1 1	30.3	2.1	22.2	2.3	19.0	31.5	1.7	31.9	25.5	3.7	23.3
3 1	33.5	2.6	28.5	3.5	28.7	1.4	0.5	1.6	3.8	1.6	3.9
5 1	13.5	2.1	4.4	2.9	2.5	3.1	1.5	2.6	3.6	2.5	2.3
7 1	40.6	4.1	71.2	10.4	62.3	69.3	7.5	64.7	95.5	11.2	78.0
9 1	14.1	2.9									
1 2	27.9	1.7	18.3	2.3	15.7	2.7	1.2	0.6	6.5	2.7	2.8
3 2	52.6	2.1	69.3	7.6	67.7	70.3	5.7	60.4	97.8	8.0	96.3
5 2	3.2	2.4	3.5	2.8	2.7						
7 2	7.4	2.1	8.4	6.5	9.3	3.9	3.9	1.6			
1 3	9.4	1.2	13.6	5.2	11.0	14.2	2.7	13.7	18.0	8.6	8.9
3 3	8.5	5.3	16.7	6.0	20.3	3.6	2.4	1.0	6.2	6.1	2.3
5 3	5.0	2.1	5.6	5.5	2.9						
7 3	15.9	2.4									
9 3	5.9	1.2									
1 4	12.1	5.0									
3 4	17.6	3.8									
5 4	3.2	1.5									
7 4	1.8	1.2									

600 Å.

The AM's were evaporated from thoroughly outgassed SAES emitters located at a distance of about 10 cm from the sample surface in order to ensure homogeneity. Auger electron spectroscopy (AES) was used to monitor the evaporation rate. The saturation of the AES signals is usually supposed to indicate the completion of 1 ML corresponding to two AM atoms per (2×1) substrate unit cell. In the case of the Na/Ge system, the evaporation rate was controlled by the intensity of the ($\frac{3}{2}$0) and ($\frac{5}{2}$0) superlattice reflections, because the Ge *LMM* and the Na *KLL* transitions overlap in the 960–990-eV regime. The Na/Ge(001)(2×1) data set was taken after the (simultaneous) saturation of the ($\frac{3}{2}$0) and the ($\frac{5}{2}$0) intensities. The (2×1) superlattice is stable upon AM adsorption; however, the LEED patterns showed a high background at AM saturation coverage, indicating some disorder. The reflection intensities were measured using the *z*-axis geometry[46] at grazing incidence slightly above the critical angle of total reflection (0.32° for $\lambda=1.541$ Å) by rotating the sample around the surface normal.[46] Using 0.8° Soller slits an out-of-plane resolution of $\Delta q_z=(5.7\times10^{-2})\cos(\alpha_f)$ Å^{-1} could be achieved which corresponds to about 0.05 reciprocal lattice units (rlu) where 1 rlu$=2\pi/c_0=2\pi/5.658$ Å$^{-1}=1.11$ Å^{-1}. The maximum beam exit angle α_f relative to the sample surface was about 56°, which corresponds to a maximum momentum transfer $q_z=4$ rlu normal to the sample surface. The adsorbate structures were found to be very stable. Within several days of data collection (important only for the rotating anode experiments) no significant intensity change and profile broadening of the control reflections could be detected.

In total, six data sets were recorded, five of them including superlattice reflection rods and consisting of about 60–90 symmetry-independent reflections. Using this huge amount of data a detailed analysis of the AM/Ge(001)(2×1) surface structures is possible. The data analysis was carried out by conventional least-squares refinement, the results are discussed in the following sections and are provided in the Appendix, Tables A1–A5. In general, the agreement between observed and calculated data is very satisfactory. Tables II and III list only the measured in-plane ($q_z=0$) structure factor intensities, $|F^{obs}|^2$ and their standard deviations σ obtained for all AM/Ge data sets as well as for the clean Ge(001)(2×1) surface taken from Ref. 50. The reflection indices are related to the (2×1) unit cell. For the AM/Ge adsorbate structures we have also added the calculated structure factor intensities, $|F^{calc}|^2$ derived for the best fit models discussed below. For better comparison, the intensities are normalized to the (3 0) reflection, which is the most intense of all cases. From the comparison of the measured intensities it is directly evident that

TABLE III. $|F^{obs}|^2$, σ, and $|F^{calc}|^2$ for K/Ge(001)(2×1) and Na/Ge(001)(2×1).

	Ge(001)(2×1) Grey *et al.* (Ref. 50)		K/Ge(001) (2×1) superstructure ≈0.30 ML Synchrotron			≈0.50 ML			Na/Ge(001) ≈0.64 ML		
hk	$\|F^{obs}\|^2$	σ	$\|F^{obs}\|^2$	σ	$\|F^{cal}\|^2$	$\|F^{obs}\|^2$	σ	$\|F^{cal}\|^2$	$\|F^{obs}\|^2$	σ	$\|F^{cal}\|^2$
1 0	45.6	1.5	24.7	2.4	26.1	7.0	0.2	7.4	11.7	2.5	13.8
3 0	100.0	1.4	100.0	5.9	99.6	100.0	4.3	98.5	100.0	6.8	109.4
5 0	2.6	1.2	2.5	1.2	1.4	5.8	1.1	4.5	6.9	0.6	7.1
7 0	4.7	2.1	7.0	4.2	5.5	1.8	0.9	1.5	2.9	1.0	3.5
9 0	1.5	1.5				2.1	1.9	3.7			
1 1	30.3	2.1	25.4	0.6	25.4	20.4	2.5	18.3	14.5	1.0	13.0
3 1	33.5	2.6	29.0	3.5	23.0	10.1	1.6	9.5	19.4	2.2	19.5
5 1	13.5	2.1	11.6	5.0	6.0	2.5	0.8	1.8	3.8	0.6	4.0
7 1	40.6	4.1	50.5	14.0	60.6	69.0	10.6	57.0	55.1	5.4	61.0
9 1	14.1	2.9	22.6	8.2	17.9				46.1	3.4	47.1
1 2	27.9	1.7	22.0	3.0	17.8	10.0	2.0	6.9	13.2	0.8	13.2
3 2	52.6	2.1	55.8	5.9	63.6	75.1	25.4	59.8	61.5	5.4	55.1
5 2	3.2	2.4	1.6	1.1	1.0	2.9	1.1	4.2	4.5	2.0	6.2
7 2	7.4	2.1				2.0	1.6	1.6			
9 2						4.0	3.1	2.9			
1 3	9.4	1.2	14.4	3.7	11.9	6.8	1.6	6.0	4.3	0.8	4.5
3 3	8.5	5.3				8.5	1.8	7.7	7.4	0.8	7.5
5 3	5.0	2.1	6.9	3.7	3.3	1.5	1.2	1.4			
7 3	15.9	2.4	25.2	5.9	35.0	26.9	7.6	32.7			
9 3	5.9	1.2				22.7	6.2	26.4	39.7	4.4	29.1
1 4	12.1	5.0	6.1	4.3	7.0						
3 4	17.6	3.8	20.2	7.5	24.8	19.7	6.6	23.7	14.8	2.3	14.1
5 4	3.2	1.5	3.3	3.3	3.9						
7 4	1.8	1.2									
1 5						2.9	3.2	2.0			
3 5						1.7	2.4	4.4	1.1	1.0	1.5

the adsorption geometry of Cs and K on Ge(001)(2×1) is coverage dependent.

III. AM/Ge(001)(2×1) STRUCTURE ANALYSES

A. The structure of Cs/Ge(001)(2×1) at half and full saturation coverage

The first step of the data analysis is the calculation of the projected Patterson function $P(u,v)$ using the in-plane data only:

$$P(u,v)=\sum_{hk}|F_{hk}^{\text{obs}}|^2\cos[2\pi(hu+kv)]\ . \tag{1}$$

Maxima in the Patterson function correspond to interatomic vectors in the structure.[46,51] As an example we show in the upper two panels of Fig. 2 the z-projected Patterson functions $P(u,v)$ calculated for the clean and

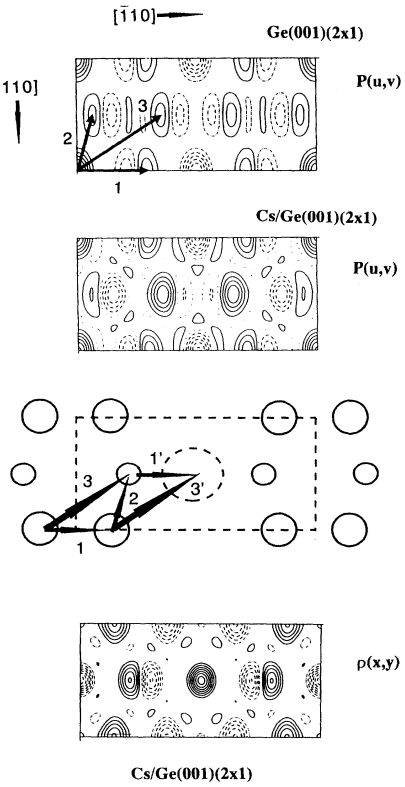

FIG. 2. Z-projected Patterson functions $P(u,v)$ of the clean and Cs-covered Ge(001)(2×1) surface at half saturation coverage normalized to the same scale. The positive maxima in the first panel (solid lines) labeled 1, 2, and 3 can be related to the corresponding interatomic Ge-Ge vectors 1, 2, and 3 of the *uncovered* Ge(001)(2×1) surface shown in the third panel. Adsorption of Cs (large dashed circle, radius not on scale) in the center of the (2×1) unit cell gives rise to new Cs-Ge vectors 1′ and 3′ whose orientations are nearly identical with 1 and 3 and therefore leading to an enhancement of the maxima 1 and 3 as shown in the second panel for $P(u,v)$ of the Cs/Ge(001) data set. The lowest panel shows the Fourier synthesis $\rho(x,y)$ of the Cs-covered surface. The positive maxima can be related to Ge atoms in the first two substrate layers and to adsorbed Cs.

the Cs-covered Ge(001)(2×1) surfaces at about half saturation coverage. In both cases three positive maxima labeled 1, 2, and 3 are observed, which are shown as solid lines. Negative maxima (dashed lines) also appear since only fractional order reflections are included in the calculation.[51] For the uncovered Ge(001)(2×1) surface the positive maxima can be related to the vectors 1, 2, and 3 between the dimer atoms (1) and between the dimer atoms and second-layer Ge atoms (2 and 3). This is indicated in the third panel of Fig. 2, which shows the (2×1)-superstructure unit cell (dashed lines) as well as the dimer and the second-layer Ge atoms by large and small solid circles, respectively. For the Cs-coverged surface the same maxima are observed in the projected Patterson function, however, with different weight (intensity), which is represented by the number of contour levels. On a qualitative approach the increased weight of the maxima 1 and 3 after Cs adsorption gives some evidence for the occupation of the position $T3$ in the center of the (2×1) unit cell. The Cs atom is represented by the large dashed circle in the third panel of Fig. 2. Due to Cs adsorption in $T3$ new vectors 1′ and 3′ between Cs and Ge atoms appear that have almost the same orientation as the Ge-Ge vectors 1 and 3. Since for the weight of a given Patterson maximum both the product of the atomic numbers, $Z_i\times Z_j$, of the atoms i and j and the multiplicity of the corresponding vector within the unit cell contribute, the maxima 1 and 3 in the Patterson function of the Cs-covered surface is enhanced relative to those derived for the clean surface. In contrast, there is no intensity change of maximum 2, since Cs adsorption does not lead to an additional contribution in this case.

The least-squares refinement using this trial structure model resulted in a weighted residuum (R_w) of 4.6% and a goodness of fit (GOF) of 1.16 (Ref. 52) if the occupation factor is refined to 0.76.[48] The lowest part of Fig. 2 shows the Fourier synthesis, $\rho(x,y)=\sum_{hk}|F_{hk}^{\text{obs}}|\cos[2\pi(hx+ky)+\alpha_{hk}^{\text{cal}}]$ of the projected structure, where α_{hk}^{cal} represents the calculated phases on the basis of the structure model. The Ge atoms as well as the Cs atom in the $T3$ position are directly evident by the positive maxima. No other Cs-adsorption sites can be observed for half Cs-saturation coverage.

Another procedure for obtaining a starting model for the structure refinement consists in the calculation of the difference Fourier synthesis $\Delta\rho(x,y)$, which in the present case is defined by

$$\Delta\rho(x,y)=\sum_{hk}(|F_{hk}^{\text{obs}}|-|F_{hk}^{\text{cal}}|)\cos[2\pi(hx+ky)-\alpha_{hk}^{\text{cal}}]\ . \tag{2}$$

In Eq. (2) F_{hk}^{cal} represents the structure factors calculated on the basis of a trial structure model. Positive (negative) maxima in $\Delta\rho(x,y)$ indicate where extra electron density must be added (subtracted) in order to describe the structure more accurately. This procedure is shown in Fig. 3 using the Cs/Ge(001)(2×1) data set *at Cs-saturation* coverage. On the left column a sequence of trial structures is shown; the corresponding difference Fourier syntheses are plotted on the right. In addition, for each plot of

$\Delta\rho(x,y)$ the residual R_w obtained for the trial structure and the contour line spacing is indicated below and above the maps, respectively. Beginning with a trial structure taking account of the Ge atoms in the first two layers only and thereby neglecting all Cs contributions a residuum of only $R_w=41\%$ is obtained indicating bad agreement between $|F^{obs}|$ and $|F^{calc}|$, as can be expected. However, the function $\Delta\rho(x,y)$ exhibits a prominent positive maximum at $T3$ pointing to an electron density deficiency due to the neglected Cs contribution (first row of Fig. 3). However, in contrast to the data set measured at half saturation coverage a structure model assuming Cs to be adsorbed in $T3$ only is found not to be completely adequate. Successively improved structure models shown in the following rows of Fig. 3 include also Cs atoms at asymmetric (a) positions labeled a-$T4$ and a-P within the (2×1) superstructure unit cell. The large circles represent Cs atoms, the numbers inside the circles indicate the occupation factors of the positions. For steric reasons ($b_0=4.000$ Å, Cs radius$=r_{Cs}\approx2.1-2.6$ Å) the simultaneous occupation of the $T3$ and the a-$T4$ positions is excluded, therefore during the structure refinement we used the following constraint for the occupancy factors θ within the unit cell: $\theta(T3)+\theta(a\text{-}T4)\leq1$. The best agreement ($R_w=6\%$) is obtained for a structure model where Cs atoms statistically occupy different positions as indicated in the lowest row of Fig. 3. In this case no significant maxima can be observed in the difference Fourier synthesis out of the noise. In summary, we obtain the following results.

(i) At saturation coverage Cs atoms occupy the position $T3$ and an asymmetric site, a-$T4$, close to the Ge-dimer dangling bonds. Strong Cs-Ge interaction and charge transfer from Cs to the Ge dangling bonds might be suspected from this observation. For low and saturation coverage the simultaneous occupation of $T3$ and a-$T4$ is observed for all investigated AM/Ge(001)(2×1) adsorbate structures (see also Sec. IV).

(ii) Some Cs ($\theta=2\times0.13$) is also adsorbed in an asymmetric position above the Ge-dimer rows (a-P). The asymmetry of this position might be due to steric reasons and/or due to bond formation with the Ge-dimer atoms. It must be noted that out of six data sets this is the only case where we have identified an AM to be adsorbed above the Ge-dimer rows. As has been pointed out by Soukiassian *et al.*[22] adsorption above the Ge dimers might be induced by surface contamination.

(iii) At about half saturation coverage only the $T3$ position is found to be occupied (see above), indicating a coverage-dependent ordering of the Cs atoms. Using

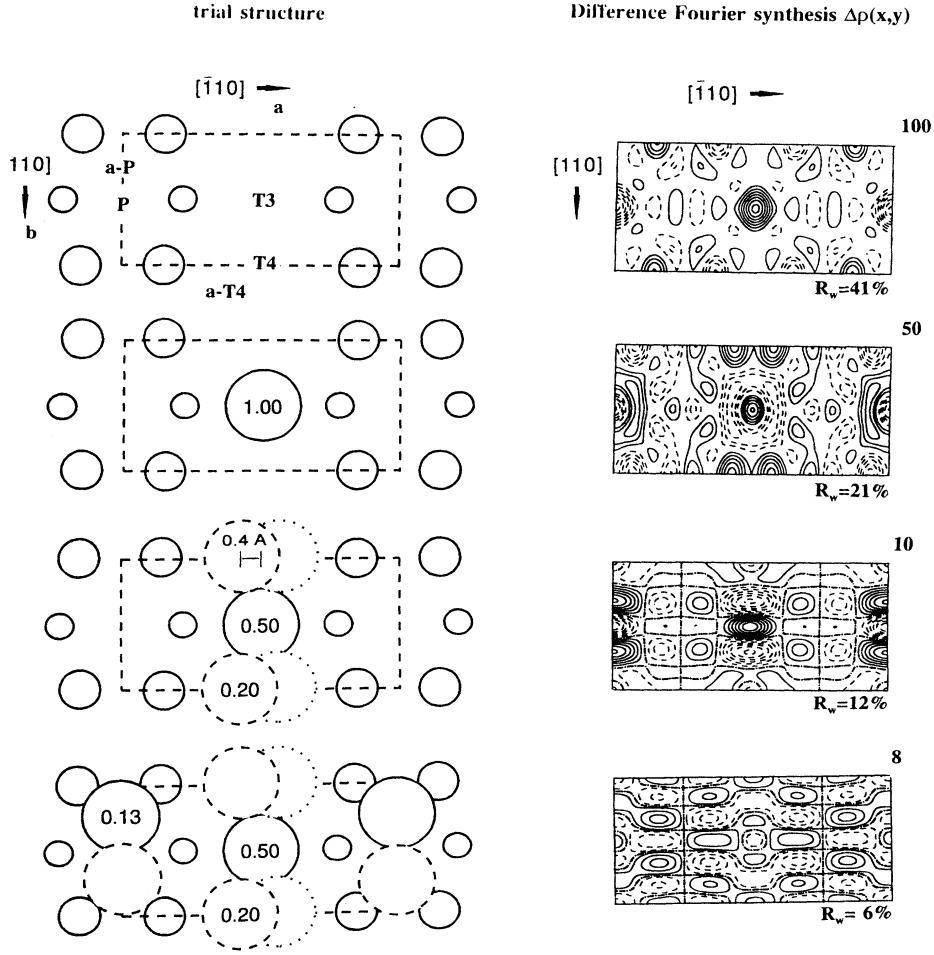

FIG. 3. Sequence of projected trial structures (left) and corresponding difference Fourier syntheses $\Delta\rho(x,y)$ (right) for Cs/Ge(001)(2×1) at Cs saturation coverage. For each structure model the weighted residuum R_w and the contour line spacing are indicated below and above the maps, respectively. Large circles represent Cs adatoms (radii not on scale). The occupancy factor θ of the adsorption sites is given by the numbers inside the circles.

STM the AM ordering at about 0.5-ML coverage leading to the formation of a one-dimensional AM chain has been observed for K/Si(001)(2×1) by Soukiassian *et al.*[22] In addition, 0.5 ML was determined as saturation coverage by the authors.

Although the basic features of the AM-adsorbate structures can be determined using the in-plane data only, a more detailed description of the structures including bond lengths and structural disorder is only possible by the analysis using the out-of-plane ($q_z \neq 0$) data. In the following we focus as a representative example on the half saturation Cs/Ge(001)(2×1) sample, where only the $T3$ position is occupied by Cs. Some results have been presented in a previous paper[48] for the half saturation data set. The results are summarized in Fig. 4 and in Table V of the Appendix, which lists the refined relative coordinates of the Cs and Ge atoms, the thermal parameters ($B = 8\pi^2 \langle u^2 \rangle$), occupancy factors, and the shifts of the Ge atoms from their bulk (1×1) positions. Figure 4 schematically shows the structure model in a projection along [110]. The solid circles represent the positions of the Ge atoms as determined for the uncovered Ge(001)(2×1) surface on the basis of our previous investigation[12] and the analysis of the integer order truncation rods.[53] The small dashed circles indicate the positions of the Ge atoms *after* Cs adsorption. Cs is represented by the large dashed circles. In accordance with the tables of the Appendix, the Ge atoms are labeled by Ge_{ij}, indicating the jth symmetrically independent atom in the ith layer. A single index (e.g., Ge_2) labels the only Ge atom in that layer. All distances are given in Å. The error bars of the distance determination are generally in the range of 0.1–0.2 Å. The Ge-Ge bond lengths are given for the structure after Cs adsorption. Several characteristic features of the structure can be summarized as follows.

(i) Large disorder normal to the sample surface is observed for both the Ge-dimer atoms and the Cs adsorbate. Without temperature-dependent measurements our experimental data cannot provide a distinction between static and dynamic disorder. A temperature-dependent measurement might rule out the unlikely possibility of a large-amplitude simple harmonic vibration of the Ge-dimer atoms and the Cs adsorbate. In Fig. 4 the disorder is taken into account by the static disorder model using "split atoms" labeled Cs_{11} and Cs_{12}, each associated with an occupancy factor of 0.38 corresponding to a total occupancy of 0.76 for the $T3$ site as discussed above and in Ref. 48. In general, partially occupied split atoms simulate the statistical distribution of the corresponding atom over different positions within the experimental coherence length. For the Ge-dimer atoms the disorder was also simulated by half occupied split atoms labeled Ge_{11} and Ge_{12}. Their separation along the z axis is about 0.80 Å. This corresponds to asymmetric Ge dimers with an inclination angle of the dimer-bonding axis of ±17.6° relative to the surface plane. In Table V both the static disorder and a dynamic disorder model using anisotropic thermal parameters is taken into account, the latter is indicated by the superscript "dyn". The Cs disorder (z separation of the split atoms 1.36 Å) might be partly induced by the Ge disorder, however, the most important contribution is expected for steric reasons since within a hard-sphere model it is not possible to locate the large Cs atoms (r_{Cs} at least 2.1–2.6 Å) along the [110] direction (lattice constant $b_0 = 4.000$ Å) at the same height level. This conclusion is supported by the results of the structure analysis on the Na/Ge(001)(2×1) system, where no such disorder along [001] is observed for the (small) Na atoms adsorbed in $T3$ (see below).

(ii) Cs adsorption does not significantly change the Ge-dimer-bonding length of 2.45 (11) Å and the dimer asymmetry. This is a general result for all AM/Ge systems investigated. In contrast, shifts of the Ge atoms in deeper layers are observed upon Cs adsorption. This is especially important for the second-layer Ge atoms, Ge_2 shifting

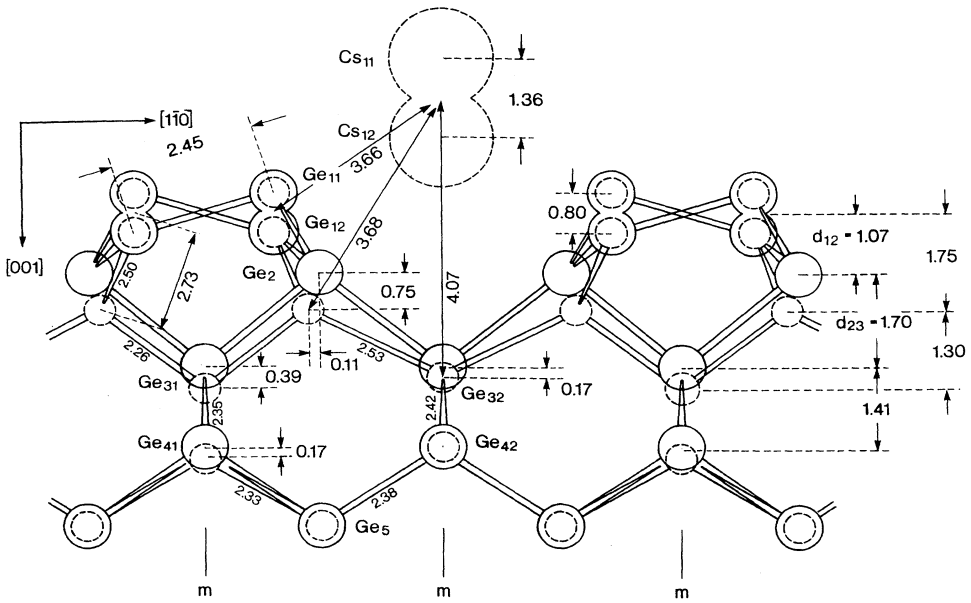

FIG. 4. Schematic view of the clean and Cs-covered Ge(001)(2×1) surface at half saturation coverage in a projection along [110]. Solid circles represent the positions of the Ge atoms as determined for the clean surface, dashed circles correspond to the structure after Cs adsorption. All distances and atomic shifts are given in Å. The Cs and Ge atoms are labeled according to Tables V–IX in the Appendix. Structural disorder along [001] is taken into account by Ge and Cs split atoms labeled Ge_{11}, Ge_{12}, Cs_{11}, and Cs_{12}. Mirror lines are indicated below.

about 0.75 Å vertically and 0.11 Å laterally (see Fig. 4). For the third-layer Ge atoms Ge_{31} and Ge_{32} vertical shifts of 0.39 and 0.17 Å are observed. Lateral shifts are forbidden by symmetry in this case. The vertical shifts lead to a change of the (average) interlayer spacings of $d_{12}=1.07$ Å and $d_{23}=1.70$ Å for the clean Ge(001) surface to $d_{12}=1.75$ Å and $d_{23}=1.30$ Å after Cs adsorption (see right part of the figure). These observations can be interpreted in terms of an interaction between the Cs atom adsorbed in $T3$ with Ge_2 and Ge_{32} (see also Sec. IV).

(iii) Two different sets of Cs-Ge bond lengths are obtained depending on what disorder model is used, the dynamic or the static disorder model. A complete overview over the bond lengths determined for all AM/Ge structures is given in Table IV. For simplicity we have indicated in Fig. 4 the *average* Cs-Ge bond lengths for the static disorder model, which correspond to the Cs-Ge bond length derived for the dynamic model within a few hundredths of an Å. The bond lengths are generally in the range between the Cs-Ge bond length found in bulk CsGe (3.58 Å) (Ref. 44) and the Cs-Ge distance[54] (3.91 Å) calculated when assuming a covalent and metallic radius for Ge and Cs, respectively. It should be noted that within the static disorder model the Cs-Ge bond lengths between the different split atoms can deviate from the average bond length by as much as ±0.6 Å (see Table IV). From crystallochemical considerations we may take the bond length as a rough estimate for the degree of interaction and the ionicity of the bond, therefore a split of the bond length of ±0.6 Å from the average bond length can be interpreted by a mixed interaction between the Cs in $T3$ and the Ge atoms Ge_2 and Ge_{32}. In contrast, the bond length from Cs to the Ge-dimer atoms is almost independent on the disorder model used.

(iv) The Ge-Ge bond lengths in both the clean and the Cs-covered structures are generally modified by at most ±8% relative to the bulk Ge-Ge bond length (2.45 Å). The only exception from this is the bond length between the Ge-dimer atoms and the second-layer Ge atom Ge_2, whose average value is 2.73 (15) Å corresponding to an expansion by +11%. This is a direct consequence of the large Ge_2 shift upon Cs adsorption.

For the Cs/Ge(001)(2×1) adsorption structure at saturation coverage the same analysis has been performed whose results are given in Table VI of the Appendix. For the $T3$-adsorbed Cs atom (Cs_1) as well as for all Ge atoms the refined structure parameters are very similar to those obtained at half Cs-saturation coverage. In addition, strong z disorder is also observed for the a-$T4$ adsorbed Cs atom, which is labeled Cs_2. The disorder of Cs_2 can also be related to steric reasons. More details are discussed in Sec. IV, which gives a summary of the AM/Ge(001)(2×1) structures.

TABLE IV. AM-Ge distances for Na, K, and Cs on the basis of the statistical and the dynamic disorder model. Theoretical AM-Ge bond lengths assuming ionic and metallic AM radii as well as bond lengths in bulk AM-Ge compounds are listed for comparison.

	Na/Ge(001) Saturation coverage	K/Ge(001) ≈0.7 saturation coverage	Cs/Ge(001) ≈0.5 saturation coverage	Cs/Ge(001) Saturation coverage
AES				
XRD coverage	0.64 ML	0.50 ML	0.38 ML	0.60 ML
		Statistical disorder model		
AM_{11}-Ge_{11}	3.18(30)[a]	3.64(20)	3.72(20)	3.76(20)
AM_{12}-Ge_{12}	3.54(30)[a]	3.70(20)	3.61(20)	3.67(20)
AM_{11}-Ge_2	3.44(35)[a]	3.65(20)	4.21(20)	4.23(20)
AM_{12}-Ge_2		3.09(20)	3.14(20)	3.24(20)
AM_{11}-Ge_{32}	4.03(35)[a]	4.30(15)	4.75(15)	4.53(15)
AM_{12}-Ge_{32}		3.56(20)	3.39(15)	3.33(20)
AM_2-Ge_{11}	2.40(30)	2.69(30)		2.97(30)
AM_2-Ge_{12}	2.73(30)	3.14(30)		3.55(30)
		Dynamic disorder model		
AM_1^{dyn}-Ge_1^{dyn}	3.35(30)[b]	3.66(20)	3.67(20)	3.70(20)
AM_1^{dyn}-Ge_2	3.44(35)	3.34(20)	3.61(20)	3.69(20)
AM_1^{dyn}-Ge_{32}	4.03(35)[b]	3.90(15)	4.01(15)	3.90(15)
AM_2^{dyn}-Ge_1^{dyn}	2.55(30)	2.91(35)		3.24(30)
		Theoretical AM-Ge bond lengths[c]		
AM metallic	3.11	3.61	3.91	
AM ionic	2.21	2.56	2.90	
Bond lengths in AM-Ge structures[d,e]	2.94	3.42	3.58	

[a]No Na-split atom.
[b]Averaged over Ge_{11} and Ge_{12}.
[c]L. Pauling, *The Nature of the Chemical Bond* (Cornell Univ. Press, Ithaca, 1960).
[d]E. Busmann, Z. Anorg. Chem. **313**, 91 (1961).
[e]J. Witte and H.G. Schnering, Z. Anorg. Chem. **327**, 260 (1964).

B. The structure of Na/Ge(001)(2×1) at Na-saturation coverage

Although the fundamental Na/Ge(001)(2×1) adsorption geometry at Na-saturation coverage is very similar to the Cs/Ge(001)(2×1) structure at Cs-saturation coverage (e.g., occupation of $T3$ and a-$T4$) some details are different, which should be addressed shortly. The differences between the structures can be attributed to the very different radii of Cs ($r^{\text{ion}}=1.67$ Å, $r^{\text{met}}=2.68$ Å) and Na ($r^{\text{ion}}=0.98$ Å, $r^{\text{met}}=1.89$ Å). In order to demonstrate the sensitivity of surface XRD for the determination of the adsorption site of a low-Z element like Na ($Z_{\text{Na}}=11$) on a heavier substrate ($Z_{\text{Ge}}=32$) we show in Fig. 5 the measured (symbols) and calculated (lines) structure factor intensities $|F_{hk}(q_z)|^2$ for the clean and the Na-covered Ge(001)(2×1) surface as a function of q_z for some superlattice rods. The intensities of the data sets are normalized to the (300) reflection. Direct comparison between the Ge(001)(2×1) and the Na/Ge(001)(2×1) data sets is possible for the (30), (11), and the (31) rods shown in the upper three panels of Fig. 5. The measured and calculated structure factor intensities $|F_{hk}(q_z)|^2$ derived for the clean Ge(001)(2×1) surface were taken from Ref. 12 and are given on the right as filled circles and solid lines, respectively. Although the fundamental features of the superlattice rods are similar, Na adsorption is found to significantly modify the reflection intensities (see also Table III for the in-plane data). In total, 66 reflections were measured for Na/Ge(001)(2×1) including seven superlattice rods. The measured and calculated structure factor intensities of the (50), (70), (12), and the (32) Na/Ge(001)(2×1) superlattice rods are shown in the lower two panels of Fig. 5. A maximum momentum

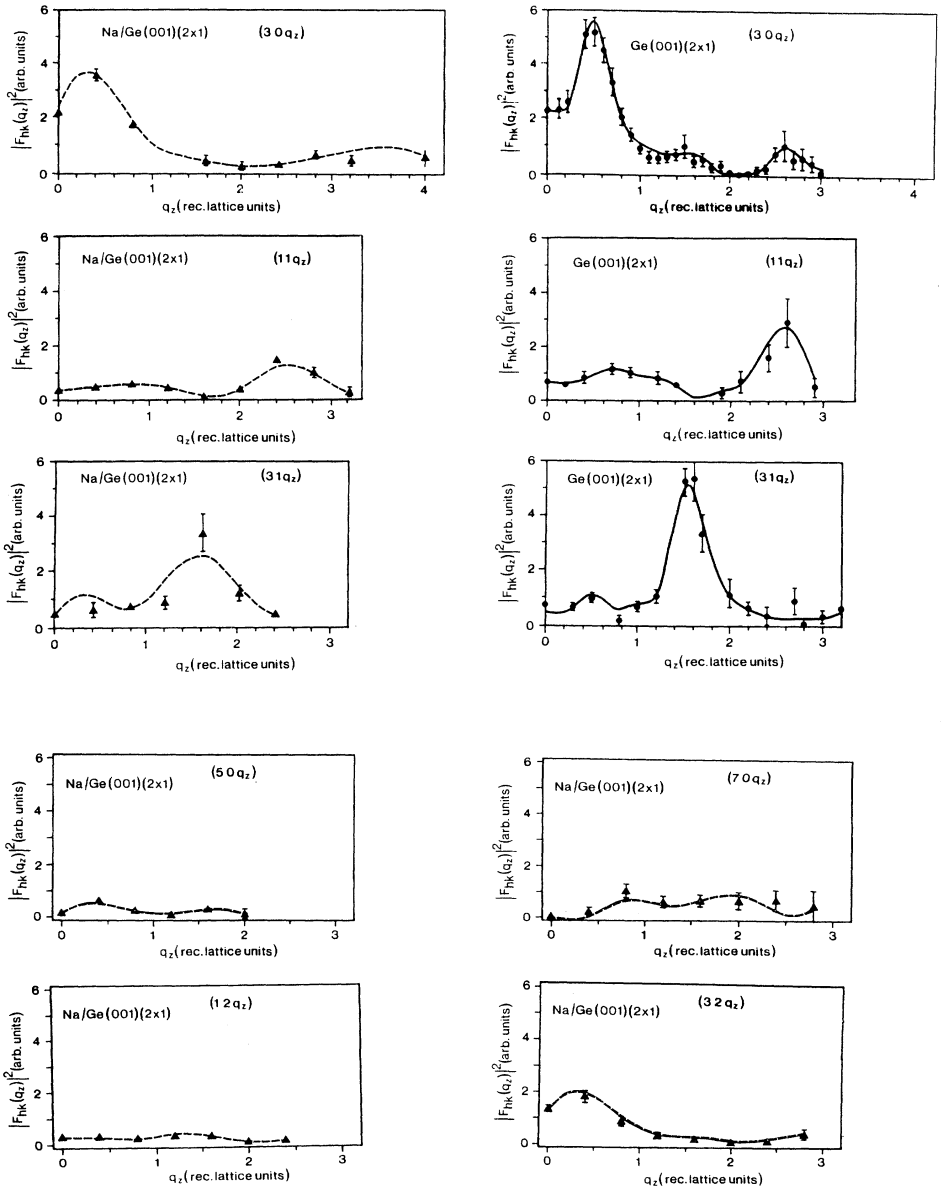

FIG. 5. Observed (symbols) and calculated (lines) structure factor intensities $|F_{hk}(q_z)|^2$ along several superlattice rods for Ge(001)(2×1) and Na/Ge(001)(2×1) at Na saturation coverage. The reflection indices are related to the (2×1) superstructure. The upper three panels give a direct comparison of the superlattice rods between Na/Ge(001)(2×1) (left) and clean Ge(001)(2×1) (right). The lower two panels show Na/Ge(001)(2×1) superlattice rods.

transfer normal to the sample surface, q_z of 4.45 $Å^{-1}$ ($\approx$4 rlu) could be achieved. This large out-of-plane data set extending to high q_z is essential for deriving accurate three-dimensional structural information. The best fit to the data (R_w=7.2%, GOF of 1.1) is obtained by a structure model whose parameters are listed in Table VII in the Appendix. A schematic view of the structure in a projection along [001] is given in Fig. 6.

The Na adsorption sites are indicated by the hatched ellipses emphasizing the pronounced in-plane disorder parallel to [110]. An in-plane disorder has not been observed for Cs/Ge(001)(2×1) and K/Ge(001)(2×1), probably due to a stronger adatom-adatom interaction between the larger AM's Cs and K. The Na disorder along [110] has been taken into account by Na split atoms (see Table VII) keeping the thermal parameters constant. There is a pronounced Na splitting along the [110] direction corresponding to the b axis of the unit cell (b_0=4.000 Å). For both Na atoms, Na_1 close to $T3$ and Na_2 in a-$T4$ it amounts to $\Delta y = \pm 0.09$ lattice units corresponding to ±0.36 Å. Along the [$\bar{1}$10] direction corresponding to the a axis of the unit cell (a_0=8.000 Å), the splitting of Na_1 from the average position (x=0.5) is within the experimental uncertainty. For Na_2 it is very large ($\Delta x = \pm 0.04 = \pm 0.32$ Å). However, it must be noted that this is characteristic for all AM/Ge(001)(2×1) adsorption systems investigated (see above) and can be attributed to the AM interaction with the Ge dangling bonds.

Another detail of the Na/Ge(001)(2×1) adsorbate structure found to be markedly different from the Cs/Ge(001)(2×1) and the K/Ge(001)(2×1) adsorbate structures is that there is no pronounced z disorder for the Na atoms. In the case of the large AM's Cs and K, the z disorder has been attributed to steric reasons. In agreement with this argument, the corrugation of the Na chains is expected to be less important. In Table VII we have also listed the shifts of the Ge atoms from their (1×1) bulk positions and from their positions determined for the clean Ge(001)(2×1) surface. There is evidence that Na adsorption has less effect on the Ge substrate than adsorption of Cs. A comparison is given on the outer right column in Table VII. Na-adsorption-induced shifts of the Ge atoms from the positions determined for the uncovered Ge(001)(2×1) surface are only Δx=0.02 Å and Δz=0.34 Å for Ge_2. For Cs/Ge(001)(2×1) we found $\Delta x = +0.11$ Å and Δz=0.75 Å. Similarly, third-layer shifts (Ge_{31} and Ge_{32}) are almost within the error bars ($\approx$0.1–0.2 Å) for Na adsorption, whereas they are 0.39 and 0.17 Å for Cs/Ge(001)(2×1).

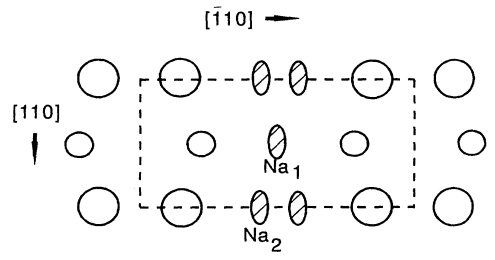

FIG. 6. Schematic view of the Na/Ge(001)(2×1) structure in the projection along [001]. The Na atoms labeled Na_1 and Na_2 are located in $T3$ and a-$T4$ (see also Figs. 1 and 3). The disorder within the surface plane is schematically represented by the diameter of the ellipses.

IV. SUMMARY OF THE XRD INVESTIGATIONS ON AM/Ge(001)(2×1)

In total, six structure analyses on the AM/Ge(001)(2×1) systems have been carried out, five of them including out-of-plane data ($q_z \neq 0$) making a three-dimensional determination of the superstructure possible. Thus, a very large amount of data has been collected. This allows a confident characterization of the AM/Ge(001)(2×1) adsorbate systems. Tables VIII and IX list the results of the structure refinements of the K/Ge(001)(2×1) structures for about 0.3- and 0.5-ML coverage, which have not been discussed so far. Generally, the structures of the adsorbate systems are similar although some differences exist in detail. Some important results are summarized in the following.

In Fig. 7 we have plotted the AM-Ge bond lengths as derived from the structure refinements. AM atoms ad-

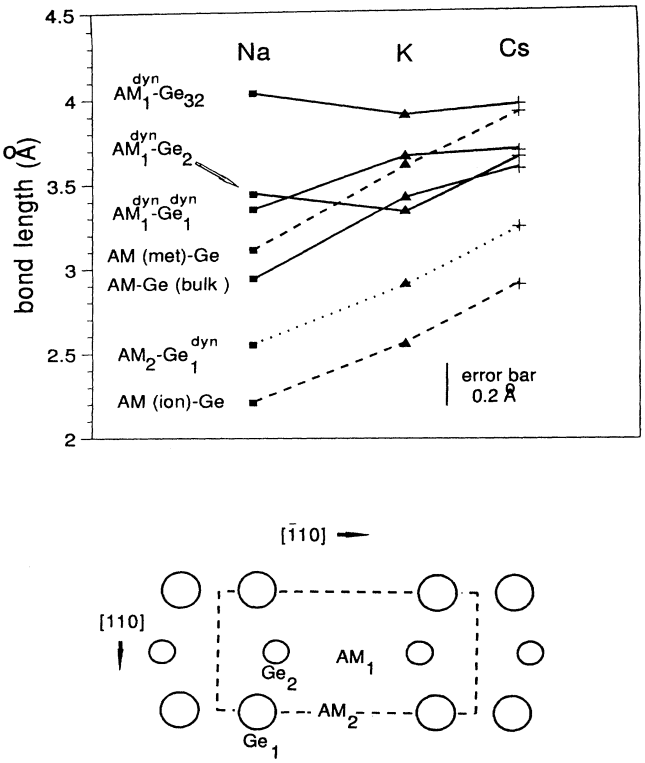

FIG. 7. AM-Ge bond lengths for Na, K, and Cs adsorbed in $T3$ and a-$T4$ on the basis of the dynamic (superscript dyn) disorder model. For comparison distances in bulk AM-Ge compounds as well as calculated bond lengths assuming metallic and ionic AM radii are indicated by AM-Ge(bulk), AM(met)-Ge, and AM(ion)-Ge. AM_1 and AM_2 label Na, K, and Cs adsorbed in $T3$ and a-$T4$, respectively, as shown in the lower part of the figure.

sorbed in the $T3$ and in a-$T4$ are labeled by AM_1 and AM_2, respectively as shown in the lower part of the figure. The bond lengths are given for the dynamic (dyn) disorder model. For comparison, we have included the (calculated) AM-Ge bond lengths assuming ionic and metallic radii of the AM atoms[54] as well as bond distances observed in bulk AMGe crystals.[44,45] In Fig. 7 this is labeled by AM(ion)-Ge, AM(met)-Ge, and AM-Ge (bulk), respectively.

The bond lengths AM_1-Ge_1 and AM_1-Ge_2 are in the regime found in bulk AM-Ge structures and are comparable with calculated AM-Ge distances if a metallic AM radius is assumed. On the other hand, the AM_2-Ge_1 bond lengths are half way between the distances that are calculated assuming an ionic AM and the bond lengths observed in bulk AM-Ge structures. Taking the bond lengths as a rough estimate of the AM-Ge interaction and the degree of charge transfer, this result can be interpreted by a mixed interaction of the AM atoms with the Ge(001)(2×1) surface. Whereas $T3$-adsorbed AM_1 atoms (on the average) only weakly interact with the Ge atoms, a significant charge transfer from the AM_2 atoms (a-$T4$) to the dangling bonds of the Ge dimers may be deduced. It should be noted that different chemisorbed states have been observed by thermal-desorption spectroscopy (TDS) for K/Si(001)(2×1) by Tanaka *et al.*,[55] although their interpretation suggesting the double-layer model $P/T3$ is in disagreement with our results.

Some modification to the structure model developed so far arises if the static disorder model is taken into account. In this case additionally a mixed interaction between AM_1 at $T3$ and the Ge atoms Ge_2 and Ge_{32} can be deduced. This is concluded by the observation that the bond lengths between the split atoms AM_{11} and AM_{12} (see Fig. 4 and Table IV) to the Ge atoms differ from the average distance by up to about ±0.6 Å. Further, two different distances between AM_2 (a-$T4$) and the Ge-dimer atoms is observed, which is due to the asymmetry of the Ge-dimer atoms represented by the split atoms Ge_{11} and Ge_{12}. In this case the longer bond (AM_2-Ge_{12}) is related to the lower-lying Ge split atom.

Chadi[56] suggested that the asymmetry of the dimers is correlated with a charge transfer from the low-lying dangling bond D_{Down} to the upper dangling bond D_{Up} leading to an empty D_{Down} and to a full D_{Up} state. Consequently, interaction and bond formation between AM_2 with the Ge dimers should be possible to D_{Down} only meaning that within this model only the longer bond distance (AM_2-Ge_{12}) is physically meaningful as schematically sketched in Fig. 8. In this case the Cs_2-Ge_{12} bond length of 3.55 (30) Å is derived, which can be related to a metallic Cs radius and suggests minor charge transfer from Cs to the dangling-bond states. This could be related to the observation that the asymmetry of the dimers (inclination angle ±17.6°) is not significantly modified by AM adsorption. It should be emphasized that since in the Bragg scattering experiments the elastic coherent part of the total scattering cross section is measured, only the average (space-time) scattering distribution is analyzed, thus making the distinction between different models (configurations) without additional information such as temperature-dependent measurements or diffuse scattering impossible.

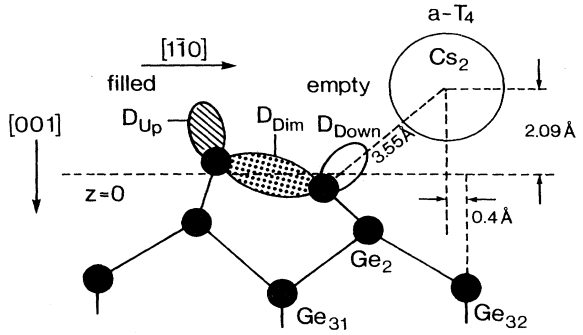

FIG. 8. Schematic view of the a-$T4$ adsorption site. The Cs atom is shifted by about 0.4 Å from the symmetric $T4$ position to the Ge dangling bond. Charge transfer is only possible into the empty D_{Down} state corresponding to a bond length of 3.55 Å (Cs_2-Ge_{12}, see also Table IV).

The second important result is the coverage-dependent occupancy factor of the different adsorption sites. This is summarized in Fig. 9 where the occupancy factors for the $T3$, a-$T4$, and the a-P sites are shown as a function of the total coverage. On the basis of the XRD structure analyses it is found that the AM-saturation coverage as determined by AES (Cs,K) or by monitoring XRD reflection intensities (Na) versus evaporation time is only 0.6–0.7 ML. This has already been proposed by Glander and Webb[57] in their LEED study of Na/Si(001)(2×1). Further, in the regime between 0.35 and 0.50 ML, we have some evidence for the preferential $T3$ occupation, whereas for low and saturation coverage both the $T3$ and the a-$T4$ site are occupied by about the same probability. The preferential $T3$-adsorption at about half AM saturation coverage can be interpreted by the formation of a one-dimensional AM chain. This has been observed for K/Si(001)(2×1) by Soukiassian using STM.[22] It can be explained by an increasing dominance of the adsorbate-adsorbate interaction over the adsorbate-substrate interaction.

Finally, we show in Fig. 10 the correlation between the metallic AM radius and the root-mean-squared (rms) vibration amplitude, $\langle u_{33}^2 \rangle^{1/2}$, of the AM atoms adsorbed in $T3$. The rms amplitude is a measure of the z disorder using the dynamic model. Although some error bars for $\langle u_{33}^2 \rangle^{1/2}$ are large, there is evidence for an increasing z disorder with increasing AM radius. This is an indication that steric reasons can account for the z disorder of the adsorbed AM's. In contrast, in the case of a pure thermal disorder a decreasing rms vibration amplitude should be expected with increasing adsorbate mass.

V. SUMMARY

In summary, we have presented a detailed surface XRD study on the structure of Na, K, and Cs adsorbed on Ge(001)(2×1) at room temperature. It could be shown that the adsorption behavior of all AM's is simi-

lar. Depending on the coverage two different adsorption sites in the large grooves between the Ge-dimer rows have been observed. At low and saturation coverage ($\approx$0.6–0.7 ML) both the *T*3 adsorption site above the third-layer Ge atoms and an asymmetric position (*a*-*T*4) close to the Ge-dimer dangling bonds were determined. There is still an apparent discrepancy between the saturation coverage determined by XRD and previous experiments, e.g., such as the medium-energy ion scattering (MEIS) experiments of Smith, Graham, and Plummer[31] who determine an absolute coverage of 0.97 and 0.98 ML for Cs and K on Si(001)(2×1), respectively. However, this discrepancy might be resolved by the consideration that XRD only probes the "coherent fraction" of AM's adsorbed in definite adsorption sites, whereas MEIS provides an integral number of adsorbed atoms independent of whether these are crystallographically ordered or not. We can speculate that due to some fraction of disordered AM atoms on the surface also in our experiments the maximum coverage might have been larger than 0.7 ML. Some evidence for disordered AM's on the surface is given by an increasing background at saturation coverage observed by LEED. On the other hand, a saturation coverage of about 1 ML with all AM's crystallographically ordered on the surface is not possible for steric reasons [AM radii and size of the (2×1) unit cell].

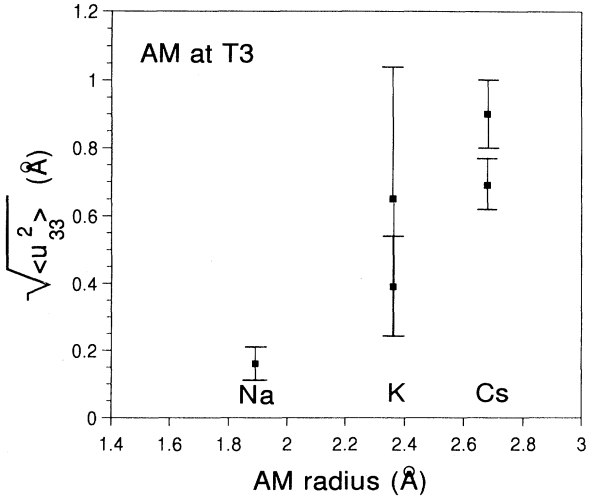

FIG. 10. Root-mean-squared vibration amplitudes along [001] vs AM radius for Na, K, and Cs adsorbed in *T*3.

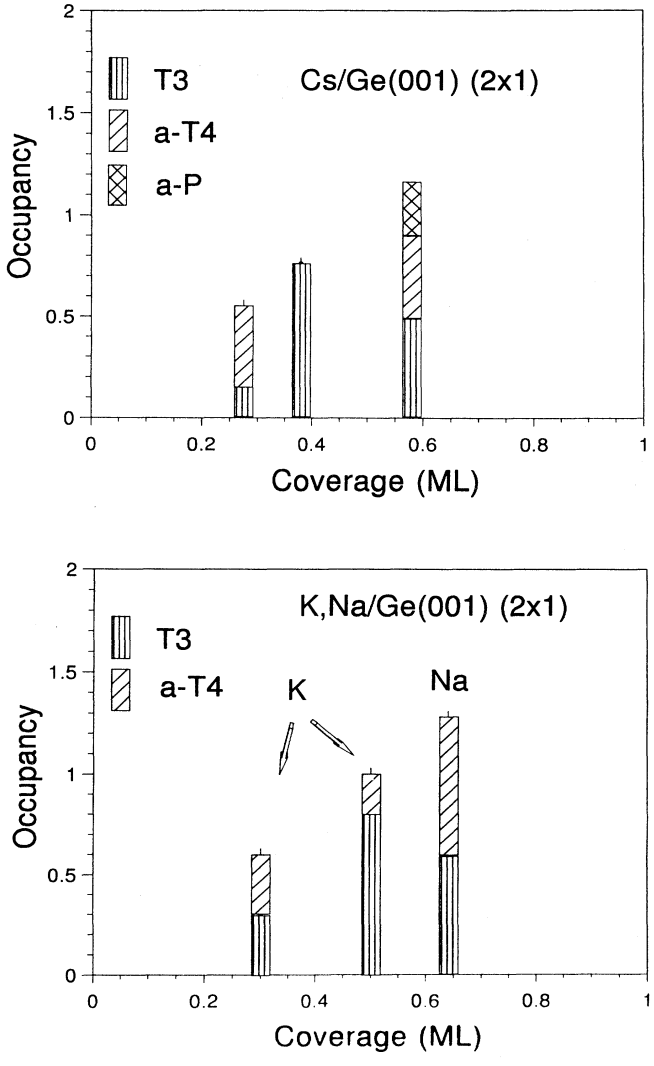

FIG. 9. Occupancy factors for Cs (upper panel), Na, and K (lower panel) for adsorption in *T*3, *a*-*T*4, and *a*-*P*.

For about half saturation coverage we have some evidence that the AM's are preferentially adsorbed in *T*3, which can be interpreted by an ordering of the AM adlayer and the formation of a one-dimensional AM chain as has been observed previously by STM. The three-dimensional analysis of the superstructure allows the determination of the AM-Ge bond lengths and the analysis of the structural disorder. Strong disorder parallel [001] is observed for the large Cs and K atoms as well as for the Ge-dimer atoms. On the basis of the present data in principle it is not possible to distinguish between dynamic and static disorder, however, the AM disorder can be attributed to steric effects, the disorder of the Ge-dimer atoms is related to the (static) asymmetry of the dimers, which is not affected by AM adsorption. As a consequence of the small Na radius a different behavior is found for the system Na/Ge(001)(2×1), where the Na disorder within the surface plane is more important than parallel [001]. On the basis of the average AM-Ge bond lengths a stronger AM-Ge interaction can be concluded for the *a*-*T*4-site-adsorbed AM's than for the *T*3-adsorbed AM's. This might be related to charge transfer from the *a*-*T*4-adsorbed AM's to the empty dangling-bond states of the Ge-dimer atoms. On the other hand, the insensitivity of the dimer asymmetry and bond length on the AM adsorption could be interpreted by a small charge transfer to the lower-lying empty dangling-bond states (D_{Down}). This picture would be consistent with a long bond length between the *a*-*T*4 adsorbed AM's and the low-lying Ge-dimer atom, which is possible within the static disorder model.

In all cases significant shifts of the Ge substrate atoms

are observed. Displacements from the bulk (1×1) positions are determined at least four layers below the surface.

ACKNOWLEDGMENTS

The authors would like to thank J. J. Csiszar for the maintenance of the rotating anode, V. Jahns, D. Wolf, J. Wever, and the workshop staff for their help at the beginning of the experiments. This work is supported by the Bundesministerium für Forschung under Technologie under Project No. 05464IAB8.

APPENDIX

Tables V–IX list the refined relative coordinates, thermal parameters ($B=8\pi^2\langle u^2\rangle$), and occupancy factors of the AM and Ge atoms within the (2×1) unit cell ($a_0=8.000$ Å, $b_0=4.000$ Å, $c_0=5.658$ Å). Parameters labeled by (*) are fixed by symmetry. The superscript dyn refers to the dynamic disorder model. Shifts of the Ge atoms ($\Delta x, \Delta z$) from their (1×1) bulk lattice sites are given in Å.

TABLE V. Cs/Ge(001)(2×1) at half saturation. 62 reflections; $R_w=10.3\%$; $R_u=12.9\%$; GOF is 1.14. (*) denotes fixed due to symmetry.

Atom	x	y	z	Thermal parameter	Δx (Å)	Δz (Å)	Occupancy
Cs_{11}	0.5(*)	0.5(*)	−0.32(2)	$B=0.6$ Å^2			0.38
Cs_{12}	0.5(*)	0.5(*)	−0.08(2)	$B=0.6$ Å^2			0.38
Cs_1^{dyn}	0.5(*)	0.5(*)	−0.19(2)	$\langle u_{11}^2\rangle^{1/2}=0.08$ Å $\langle u_{22}^2\rangle^{1/2}=0.08$ Å $\langle u_{33}^2\rangle^{1/2}=0.90(10)$ Å			0.76
Ge_{11}	0.15(1)	0.0(*)	−0.07(2)	$B=0.6$ Å^2	−0.80(8)	−0.39(10)	0.50
Ge_{12}	0.14(1)	0.0(*)	0.07(2)	$B=0.6$ Å^2	−0.88(8)	0.39(10)	0.50
Ge_1^{dyn}	0.14(1)	0.0(*)	0.00(*)	$\langle u_{11}^2\rangle^{1/2}=0.08$ Å $\langle u_{22}^2\rangle^{1/2}=0.08$ Å $\langle u_{33}^2\rangle^{1/2}=0.46(5)$ Å	−0.88(8)		1.00
Ge_2	0.22(1)	0.5(*)	0.31(3)	$B=0.6$ Å^2	−0.24(8)	0.34(16)	1.00
Ge_{31}	0.00(*)	0.5(*)	0.56(3)	$B=0.6$ Å^2	0.00(*)	0.34(17)	1.00
Ge_{32}	0.50(*)	0.5(*)	0.52(3)	$B=0.6$ Å^2	0.00(*)	0.11(11)	1.00
Ge_{41}	0.00(*)	0.0(*)	0.78(5)	$B=0.6$ Å^2	0.00(*)	0.17(30)	1.00
Ge_{42}	0.50(*)	0.0(*)	0.76(5)	$B=0.6$ Å^2	0.00(*)	0.06(30)	1.00
Ge_5	0.25(1)	0.0(*)	0.99(8)	$B=0.6$ Å^2	0.00(8)	−0.06(45)	1.00

TABLE VI. Cs/Ge(001)(2×1) at saturation coverage. 91 reflections; $R_w=10.7\%$; $R_u=11.7\%$; GOF is 1.03. (*) denotes fixed due to symmetry.

Atom	x	y	z	Thermal parameter	Δx (Å)	Δz (Å)	Occupancy
Cs_{11}	0.5(*)	0.5(*)	−0.32(2)	$B=0.6$ Å^2			0.25
Cs_{12}	0.5(*)	0.5(*)	−0.11(2)	$B=0.6$ Å^2			0.25
Cs_1^{dyn}	0.5(*)	0.5(*)	−0.21(2)	$\langle u_{11}^2\rangle^{1/2}=0.08$ Å $\langle u_{22}^2\rangle^{1/2}=0.08$ Å $\langle u_{33}^2\rangle^{1/2}=0.69(7)$ Å			0.50
Cs_2	0.45(2)	0.0(*)	−0.37(4)	$\langle u_{11}^2\rangle^{1/2}=0.41$ Å $\langle u_{22}^2\rangle^{1/2}=0.41$ Å $\langle u_{33}^2\rangle^{1/2}=1.20$ (50) Å			0.20
Cs_3	0.00	0.24(3)	−0.68(4)	$B=4.3$ Å^2			0.13
Ge_{11}	0.14(1)	0.0(*)	−0.08(2)	$B=0.6$ Å^2	−0.88(8)	−0.45(10)	0.50
Ge_{12}	0.14(1)	0.0(*)	0.08(2)	$B=0.6$ Å^2	−0.88(8)	0.45(10)	0.50
Ge_1^{dyn}	0.14(1)	0.0(*)	0.00(*)	$\langle u_{11}^2\rangle^{1/2}=0.08$ Å $\langle u_{11}^2\rangle^{1/2}=0.08$ Å $\langle u_{22}^2\rangle^{1/2}=0.59$ (4) Å	−0.88(8)	0.00(*)	1.00
Ge_2	0.24(1)	0.5(*)	0.33(3)	$B=0.6$ Å^2	−0.08(8)	0.45(15)	1.00
Ge_{31}	0.00(*)	0.5(*)	0.54(3)	$B=0.6$ Å^2	0.00(*)	0.23(17)	1.00
Ge_{32}	0.50(*)	0.5(*)	0.48(2)	$B=0.6$ Å^2	0.00(*)	−0.11(11)	1.00
Ge_{41}	0.00(*)	0.0(*)	0.80(5)	$B=0.6$ Å^2	0.00(*)	0.28(30)	1.00
Ge_{42}	0.50(*)	0.0(*)	0.79(5)	$B=0.6$ Å^2	0.00(*)	0.23(30)	1.00

TABLE VII. Na/Ge(001)(2×1). 66 reflections; $R_w=7.2\%$; $R_u=10.4\%$; GOF is 1.14. (*) denotes fixed due to symmetry.

Atom	x	y	z	Thermal parameter	Δx (Å) from bulk (1×1)	Δz (Å) from bulk (1×1)	Occupancy	Δx (Å) from clean (2×1)	Δz (Å) from clean (2×1)
Na_1	0.48(3)	0.41(3)	−0.25(3)	$B=2.0$ (1.1)			0.15		
Na_2	0.46(2)	0.09(2)	−0.14(4)	$B=4.0$ (2.4)			0.17		
Ge_{11}	0.17(1)	0.0(*)	−0.05(1)	$B=0.6$	−0.64(8)	−0.28(6)	0.50		
Ge_{12}	0.15(1)	0.0(*)	0.05(1)	$B=0.6$	−0.80(8)	0.28(6)	0.50		
Ge_2	0.24(1)	0.5(*)	0.25(2)	$B=0.6$	−0.08(8)	±0.00(11)	1.00	+0.02	+0.34
								+0.11	+0.75 (Cs)
Ge_{31}	0.00(*)	0.5(*)	0.50(2)	$B=0.6$	0.00(*)	±0.00(11)	1.00		−0.06
									+0.39 (Cs)
Ge_{32}	0.50(*)	0.5(*)	0.46(2)	$B=0.6$	0.00(*)	−0.23(11)	1.00		−0.17
									+0.17 (Cs)
Ge_{41}	0.00(*)	0.0(*)	0.74(3)	$B=0.6$	0.00(*)	−0.06(17)	1.00		
Ge_{42}	0.50(*)	0.0(*)	0.71(5)	$B=0.6$	0.00(*)	−0.23(30)	1.00		

TABLE VIII. K/Ge(001)(2×1) at 0.3-ML coverage. 64 reflections; $R_w=7.3\%$; $R_u=11.8\%$; GOF is 1.10. (*) denotes fixed due to symmetry.

Atom	x	y	z	Thermal parameter	Δx (Å)	Δz (Å)	Occupancy
K_{11}	0.5(*)	0.5(*)	−0.32(3)	$\langle u_{11}^2\rangle^{1/2}=0.20(5)$ Å $\langle u_{22}^2\rangle^{1/2}=0.28(7)$ Å $\langle u_{33}^2\rangle^{1/2}=0.08$ Å			0.40
K_{12}	0.5(*)	0.5(*)	−0.19(3)	$\langle u_{11}^2\rangle^{1/2}=0.20(5)$ Å $\langle u_{22}^2\rangle^{1/2}=0.28(7)$ Å $\langle u_{33}^2\rangle^{1/2}=0.08$ Å			0.40
K_1^{dyn}	0.5(*)	0.5(*)	−0.25(2)	$\langle u_{11}^2\rangle^{1/2}=0.19(6)$ Å $\langle u_{22}^2\rangle^{1/2}=0.26(7)$ Å $\langle u_{33}^2\rangle^{1/2}=0.39(16)$ Å			0.80
K_2	0.46(3)	0.0(*)	−0.29(4)	$B=1.20$ Å^2			0.10
Ge_{11}	0.17(1)	0.0(*)	−0.05(1)	$B=0.6$	−0.64(8)	−0.28(6)	0.50
Ge_{12}	0.15(1)	0.0(*)	0.05(1)	$B=0.6$	−0.80(8)	0.28(6)	0.50
Ge_1^{dyn}	0.16(1)	0.0(*)	0.00(*)	$\langle u_{11}^2\rangle^{1/2}=0.07(5)$ Å $\langle u_{11}^2\rangle^{1/2}=0.05(4)$ Å $\langle u_{22}^2\rangle^{1/2}=0.32(4)$ Å			1.00
Ge_2	0.23(1)	0.5(*)	0.20(2)	$B=0.6$	−0.16(8)	−0.28(11)	1.00
Ge_{31}	0.00(*)	0.5(*)	0.49(2)	$B=0.6$	0.00(*)	−0.06(10)	1.00
Ge_{32}	0.50(*)	0.5(*)	0.44(2)	$B=0.6$	0.00(*)	−0.34(11)	1.00
Ge_{41}	0.00(*)	0.0(*)	0.72(3)	$B=0.6$	0.00(*)	−0.17(17)	1.00
Ge_{42}	0.50(*)	0.0(*)	0.69(5)	$B=0.6$	0.00(*)	−0.34(30)	1.00
Ge_5	0.26(1)	0.0(*)	0.97(3)	$B=0.6$	0.06(6)	−0.17(17)	1.00

TABLE IX. K/Ge(001)(2×1) at 0.5-ML coverage. 83 reflections; $R_w=7.4\%$; $R_u=15.6\%$; GOF is 1.22. (*) denotes fixed due to symmetry.

Atom	x	y	z	Thermal parameter	Δx (Å)	Δz (Å)	Occupancy
K_1^{dyn}	0.5(*)	0.5(*)	−0.27(4)	$\langle u_{11}^2\rangle^{1/2}=0.10$ Å $\langle u_{22}^2\rangle^{1/2}=0.10$ Å $\langle u_{33}^2\rangle^{1/2}=0.65(40)$ Å			0.30
K_2	0.41(5)	0.0(*)	−0.31(5)	$\langle u^2\rangle^{1/2}=0.55(30)$ Å			0.15
Ge_1^{dyn}	0.15(1)	0.0(*)	0.00(*)	$\langle u_{11}^2\rangle^{1/2}=0.11(3)$ Å $\langle u_{22}^2\rangle^{1/2}=0.09(3)$ Å $\langle u_{33}^2\rangle^{1/2}=0.48(3)$ Å	−0.80(8)	0.00(*)	1.00
Ge_2	0.24(1)	0.5(*)	0.20(1)	$B=0.6$ Å^2	−0.08(8)	−0.28(5)	1.00
Ge_{31}	0.00(*)	0.5(*)	0.49(2)	$B=0.6$ Å^2	0.00(*)	−0.06(10)	1.00
Ge_{32}	0.50(*)	0.5(*)	0.46(2)	$B=0.6$ Å^2	0.00(*)	−0.23(10)	1.00
Ge_{41}	0.00(*)	0.0(*)	0.73(2)	$B=0.6$ Å^2	0.00(*)	−0.10(10)	1.00
Ge_{42}	0.50(*)	0.0(*)	0.71(3)	$B=0.6$ Å^2	0.00(*)	−0.23(17)	1.00
Ge_5	0.25(1)	0.0(*)	0.95(4)	$B=0.6$ Å^2	0.00(8)	−0.28(23)	1.00

[1]*Physics and Chemistry of Alkali Metal Adsorption,* edited by H. P. Bonzel, A. M. Bradshaw, and G. Ertl (Elsevier, Amsterdam, 1989).
[2]T. Aruga and Y. Murata, Prog. Surf. Sci. **31**, 61 (1990).
[3]*The Chemical Physics of Solid Surfaces and Heterogeneous Catalysis,* edited by D. A. King and D. P. Woodruff (Elsevier, New York, 1983), Vol. 3.
[4]R. W. Gurney, Phys. Rev. **47**, 479 (1935).
[5]D. M. Riffe, G. K. Wertheim, and P. H. Citrin, Phys. Rev. Lett. **69**, 571 (1990).
[6]H. Ishida and K. Terakura, Phys. Rev. B **38**, 5752 (1988).
[7]H. Ishida, Phys. Rev. B **42**, 10 899 (1990).
[8]M. Scheffler, C. Droste, A. Fleszar, F. Màca, G. Wachuta, and G. Barzel, Physica (Amsterdam) **172B**, 143 (1991).
[9]G. Pacchioni and P. S. Bagus, Surf. Sci. **269/270**, 669 (1992).
[10]G. Pacchioni and P.S. Bagus, Surf. Sci. **286**, 317 (1993).
[11]J. A. Kubby, J. E. Griffith, R. S. Becker, and J. S. Vickers, Phys. Rev. B **36**, 6079 (1987).
[12]R. Rossmann, H. L. Meyerheim, V. Jahns, J. Wever, W. Moritz, D.Wolf, D. Dornisch, and H. Schulz, Surf. Sci. **279**, 199 (1992).
[13]J. Dabrowski and M. Scheffler, Appl. Surf. Sci. **56-58**, 15 (1992).
[14]P. Krüger and J. Pollmann, Phys. Rev. Lett. **74**, 1155 (1995).
[15]J. D. Levine, Surf. Sci. **34**, 90 (1973).
[16]C. M. Wei, H. Huang, S. Y. Tong, G. S. Glander, and M. B. Webb, Phys. Rev. B **42**, 11 284 (1990).
[17]T. Urano, Y. Uchida, S. Hongo, and T. Kanaji, Surf. Sci. **242**, 39 (1991).
[18]T. Urano, S. Hongo, and T. Kanaji, Surf. Sci. **287/288**, 294 (1993).
[19]T. Abukawa, T. Kashiwakura, T. Okane, Y. Sasaki, T. Takahashi, Y. Enta, S. Suzuki, S. Kono, S. Sato, T. Kinoshita, A. Kakizati, T. Ishii, C. Y. Park, S. W. Yu, K. Sakamoto, and T. Sakamoto, Surf. Sci. **261**, 217 (1992).
[20]Y. Enta, S. Suzuki, S. Kono, and T. Sakamoto, Phys. Rev. B **39**, 5524 (1989).
[21]T. Abukawa and S. Kono, Phys. Rev. B **37**, 9097 (1988).
[22]P. Soukiassian, J. A. Kubby, P. Mangat, Z. Hurych, and K. M. Schirm, Phys. Rev. B **46**, 13 471 (1992).
[23]Y. Hasegawa, I. Kamiya, T. Hashizume, T. Sakurai, H. Tochihara, M. Kubota, and Y. Murata, Phys. Rev. B **41**, 9688 (1990).
[24]E. G. Michel, P. Pervan, G. R. Castro, R. Miranda, and K. Wandelt, Phys. Rev. B **45**, 11 811 (1992).
[25]V. Eteläniemi, E. G. Michel, and G. Materlik, Surf. Sci. **251/252**, 483 (1991).
[26]A. Lessmann, Ph.D. thesis, University Hamburg, 1993.
[27]M. C. Asensio, E. G. Michel, J. Alvarez, C. Ocal, R. Miranda, and S. Ferrer, Surf. Sci. **211/212**, 31 (1989).
[28]T. Hashizume, I. Sumita, Y. Murata, S. Hoydo, and T. Sakurai, J. Vac. Sci. Technol. B **9**, 742 (1991).
[29]T. Hashizume, Y. Hasegawa, I. Kamiya, T. Ide, I. Sumita, S. Hoydo, T. Sakurai, H. Tochihara, M. Kubota, and Y. Murata, J. Vac. Sci. Technol. A **8**, 233 (1990).
[30]T. Makita, S. Kohmoto, and A. Ichimiya, Surf. Sci. **242**, 65 (1991).
[31]A. J. Smith, W. R. Graham, and E. W. Plummer, Surf. Sci. Lett. **243**, L37 (1991).
[32]L. Spiess, P.S. Mangat, S.-P. Tang, K. M. Schirm, A. J. Freeman, and P. Soukiassian, Surf. Sci. Lett. **289**, L631 (1993).
[33]S. Ciraci and I. P. Batra, Phys. Rev. B **37**, 2955 (1988).
[34]R. Ramirez, Phys. Rev. B **40** 3962 (1989).
[35]Ye Ling, A. J. Freeman, and B. Delley, Phys. Rev. B **39**, 10 144 (1989).
[36]I. P. Batra, J. Vac. Sci. Technol. A **8**, 3425 (1990).
[37]K. Kobayashi, Y. Morikawa, K. Terakura, and S. Blügel, Phys. Rev. B **45**, 3469 (1992).
[38]Y. Morikawa, K. Kobayashi, and K. Terakura, Surf. Sci. **283**, 377 (1993).
[39]Y. Morikawa, K. Kobayashi, T. Terakura, and S. Blügel, Phys. Rev. B **44**, 3459 (1991).
[40]E. M. Oellig and R. Miranda, Surf. Sci. Lett. **177**, L947 (1986).
[41]J. E. Ortega, E. M. Oellig, J. Ferrón, and R. Miranda, Phys. Rev. B **36**, 6213 (1987).
[42]A. J. Smith, W. R. Graham, and E. W. Plummer, Surf. Sci. Lett. **243**, L37 (1991).
[43]D.-S. Lin, T. Miller, and T.-C.Chiang, Phys. Rev. B **44**, 10 719 (1991).
[44]E. Busmann, Z. Anorg. Chem. **313**, 91 (1961).
[45]J. Gallmeier, H. Schäfer, and A. Weiß, Z. Naturforsch. Teil B **24**, 665 (1969).
[46]R. Feidenhans'l, Surf. Sci. Rep. **10**, 105 (1989); I. K. Robinson, in *Handbook of Synchrotron Radiation,* edited by G. S. Brown and D. E. Moncton (Elsevier, Amsterdam, 1991), Band III.
[47]F. Kretschmar, D. Wolf, H. Schulz, H. Huber, and H. Plöckl, Z. Kristallogr. Mineral. **178**, 130 (1987).
[48]H. L. Meyerheim and R. Sawitzki, Surf. Sci. Lett. **301**, L203 (1994).
[49]We use a sample setting corresponding to a primitive (p) (1×1) surface unit cell which is related to the face (f) centered setting by $[100]_p=0.5\{[100]_f+[010]_f\}$, $[010]_p=0.5\{[100]_f-[010]_f\}$, and $[001]_p=[001]_f$. The lattice constants of the (2×1) superstructure unit cell are $a_0=8.000$ Å, $b_0=4.000$ Å, $c_0=5.658$ Å.
[50]F. Grey, R. L. Johnson, J. S. Pedersen, R. Feidenhans'l, and M. Nielsen, in *The Structure of Surfaces II,* edited by J. F. van der Veen and M. von Hove, Springer Series in Surface Sciences Vol. 11 (Springer, Berlin, 1988).
[51]M. J. Buerger, *Vector Space and its Applications in Crystal Structure Investigations* (Wiley, New York, 1959).
[52]The residua are given by $R_u=\sum_{hkl}||F^{obs}_{hkl}|-|F^{calc}_{hkl}||/\sum_{hkl}|F^{obs}_{hkl}|$ and $R_w=(\sum_{hkl}w_{hkl}||F^{obs}_{hkl}|-|F^{calc}_{hkl}||^2/\sum_{hkl}w_{hkl}|F^{obs}_{hkl}|^2)^{1/2}$, with $w_{hkl}=\sigma^{-2}_{hkl}$ and GOF$=(N-p)^{-1}\sum_{hkl}(||F^{obs}_{hkl}|-|F^{calc}_{hkl}||^2/\sigma^2_{hkl})$, where N is the number of reflections and p the number of free parameters.
[53]H. L. Meyerheim, Habilitation thesis, University Munich, 1994.
[54]L. Pauling, *The Nature of the Chemical Bond,* 3rd ed. (Cornell University Press, Ithaca, 1960); R. D. Shannon and T. C. Prewitt, Acta Crystallogr. Sect. B **25**, 925 (1969).
[55]S. Tanaka, N. Takagi, N. Minami, and M. Nishijima, Phys. Rev. B **42**, 1868 (1990).
[56]D. J. Chadi, Phys. Rev. Lett. **43**, 43 (1979).
[57]G. S. Glander and M. B. Webb, Surf. Sci. **222**, 64 (1989).